Physica Medica 86 (2021) 82–90

Contents lists available at ScienceDirect

Physica Medica

journal homepage: www.elsevier.com/locate/ejmp

Original paper

Use of genetic algorithm for PTV optimization in single isocenter multiple metastases radiosurgery treatments with Brainlab Elements™

José Alejandro Rojas-López *, Rogelio Manuel Díaz Moreno, Carlos Daniel Venencia

Instituto Zunino, Obispo Oro 423, 5000 Córdoba, Argentina

ARTICLE INFO

Keywords:
Radiosurgery
Multiple metastases
Optimized PTV margin
Genetic algorithm

ABSTRACT

Purpose: To optimize PTV margins for single isocenter multiple metastases stereotactic radiosurgery through a genetic algorithm (GA) that determines the maximum effective displacement of each target (GTV) due to rotations.

Method: 10 plans were optimized. The plans were created with Elements Multiple Mets™ (Brainlab AG, Munchen, Germany) from a predefined template. The mean number of metastases per plan was 5 ± 2 [3,9] and the mean volume of GTV was 1.1 ± 1.3 cc [0.02, 5.1]. PTV margin criterion was based on GTV-isocenter distance and target dimensions. The effective displacement to perform specific rotational combination (roll, pitch, yaw) was optimized by GA. The original plans were re-calculated using the PTV optimized margin and new dosimetric variations were obtained. The D_{mean}, D_{99}, Paddick conformity index (PCI), gradient index (GI) and dose variations in healthy brain were studied.

Results: Regarding targets located shorter than 50 mm from the isocenter, the maximum calculated displacement was 2.5 mm. The differences between both PTV margin criteria were statistically significant for D_{mean} ($p = 0.0163$), D_{99} ($p = 0.0439$), PCI ($p = 0.0242$), GI ($p = 0.0160$) and for healthy brain V_{12} ($p = 0.0218$) and V_{10} ($p = 0.0264$).

Conclusion: The GA allows to determine an optimized PTV margin based on the maximum displacement. Optimized PTV margins reduce the detriment of dosimetric parameters. Greater PTV margins are associated with an increase in healthy brain volume.

1. Introduction

Stereotactic radiosurgery (SRS) of multiple metastases has become a commonly used technique in recent years [1–3]. SRS treatments have steadily improved, with associated benefits for patient's survival increase and local control from 70% to 90% [1,4–6].

In SRS treatment with multiple metastases, the use of an isocenter for each target or a single isocenter for all targets can be chosen [7–10]. The advantages of a single isocenter are that treatments are carried out in less time, conformity index is improved, gradient index (GI) decreases and the setup uncertainties are reduced [11]. However, the main disadvantage is that the isocenter may not necessarily be located near to the targets [7]. In single isocenter for multiple metastases SRS (SIMM-SRS), setup accuracy is strategic because it is essential to locate correctly the isocenter and to positionate the targets where they should be [12–14]. A variety of stereotactic frameless systems have been proposed to reduce setup uncertainties. These systems include corrections in 6 dimensions with translations in 3 dimensions (3D) and isocentric rotations in 3 dimensions (roll, pitch and yaw) by means of robotic table [20]. However, the dosimetric impact of setup errors due to 3D rotations has been analyzed in few studies [15–27].

Setup uncertainties can generate degradations of the dose distribution [10–11,15]. These uncertainties depend on factors such as the volume, shape and relative position of the lesion with respect to the isocenter [16,17]. Defining sufficient margins to ensure coverage of the planning target volumes (PTV) is a solution, but it can entail an overdose impact in organs at risk (OAR) and healthy brain [18–20]. A 1 mm margin to the PTV has been proposed to ensure enough coverage for the distribution of setup errors and improve local recurrence for targets up to 8 cm from the isocenter [14,23,24].

A widespread way to study the dosimetric impact due to discrepancies between the original plan and actual treatment setup is based

* Corresponding author.
E-mail addresses: alexrojas@ciencias.unam.mx (J.A. Rojas-López), rdiaz@institutozunino.org (R.M. Díaz Moreno), dvenencia@institutozunino.org (C.D. Venencia).

https://doi.org/10.1016/j.ejmp.2021.05.031
Received 4 March 2021; Received in revised form 15 May 2021; Accepted 22 May 2021
Available online 29 May 2021

upon the 6D displacements simulation of the target from the set of reference images. Dosimetric variations have been related as a function of the effective target displacement [25–29]. For example, one method recalculates dose from the displaced anatomy and the plan with the original parameters [19]. Another approach is to shift the original plan dose distribution matrix relative to the fixed anatomy [9,30]. Calculation equivalence of both methods was demonstrated [25]. If displacements are relatively small with respect to the relevant anatomical dimensions and the radiological path of the treatment beams towards the targets, this approach is valid for an arc treatment [25]. Either way, the potential GTV dosimetric detriment can be assessed and suitable PTV margins can be suggested to improve results.

The dosimetric impact of setup errors due to rotations in a SIMM-SRS plan must be studied considering the order in which the displacements are performed [31]. The effect of translational displacements in SIMM-SRS was studied by Hosang et al. [20]. Translational displacements are associated with rigid and commutative transformations. The impact of translations in the final position are included in PTV margins. On the other hand, in rotations this does not happen. The effect of rotation is more noticeable while the target is farther from the isocenter. This is due to the fact that the greater the distance to isocenter, the greater the GTV arc path. The set of transformations associated with isocentric rotations has a matrix representation and satisfies the preservation of the origin, the Euclidean distance and the orientation. However, this set of transformations is non-commutative, therefore the final position of the displaced target is affected by the order and direction in which the rotations are carried out [26,32] as shown in Fig. 1. If three rotations (roll, pitch, yaw) and the direction (clockwise, counterclockwise) are considered, there are 48 possible combinations. Therefore, the study of which is the biggest displacement applying rotations in a certain order and direction constitutes an optimization problem.

An established technique to solve problems of this type are differentiated evolution algorithms and genetic algorithms (GA) [33]. GA are heuristic optimization techniques inspired by the principle of Darwinian natural evolution [33,34]. Currently, these algorithms have been successfully applied in a wide variety of problems that include areas such as heart disease diagnosis [35], facial recognition [36], designing telecommunications sensors [37] and association between patient survival and radiological data in radiotherapy [38].

In this work, the rotational combination that provides the maximum and minimum effective gross tumor volume (GTV) displacement in a SIMM-SRS was determined through a classic GA. A given margin to the PTV was proposed to cover the GTV considering the maximum displacements. Plans were recalculated with the new PTV and the GTV potential dosimetric detriment was reevaluated and compared to that of the plans with the old PTV and same maximum displacements.

2. Materials and methods

A TrueBeam STx® high precision linear accelerator (Varian Medical Systems, Palo Alto, CA) was used. It has energies of 6 and 10 MV with and without a flattening filter and a high definition multileaf collimator (HDMLC). The HDMLC has 120 slides with 60 central pairs of slides 2.5 mm wide at the isocenter [39]. TrueBeam STx® features portal MV imaging, kV planar imaging, cone beam CT, an ExacTrac® version 6.0 system (Brainlab AG, Munchen, Germany) based on bone fusion with 0.5°/0.5 mm tolerances, and a Perfect Pitch 6D robotics table [40]. The system has software for automatic image registration and remote patient positioning.

2.1. Treatment planning

Brainlab Elements™ v.2.0 (Brainlab AG, Munchen, Germany) is a commercial treatment planning system (TPS) that automatically optimizes a dedicated set of dynamic arcs to treat single isocenter brain lesions [41,42]. The beams of the Elements™ plans are selected from a predefined set of templates with a range of 5 table angles of 0, 20, 60, 280 and 320 degrees. The initial gantry angles correspond by default to the intervals of 190°–350° for the table between 20°–60° and 10°–170° for the table between 0°–280°.

In this work, SIMM-SRS plans were optimized for the TrueBeam STx® accelerator with HDMLC using 6 MV energy with a flattening filter. Dose calculation was performed with a 1 mm grid using the Brainlab pencil beam algorithm [43–45]. The plans were created from a predefined set of templates for a single fraction with 95% coverage of the prescribed dose at 100% PTV with the 90% tolerance coverage. A standard set of constraints for OARs was applied based on the predefined template considering the cochlea, the lens, the eyes, the optic nerve, the optic tract, the chiasm and the healthy brain. The healthy brain was defined as the volume of the brain minus the volumes of the GTVs and

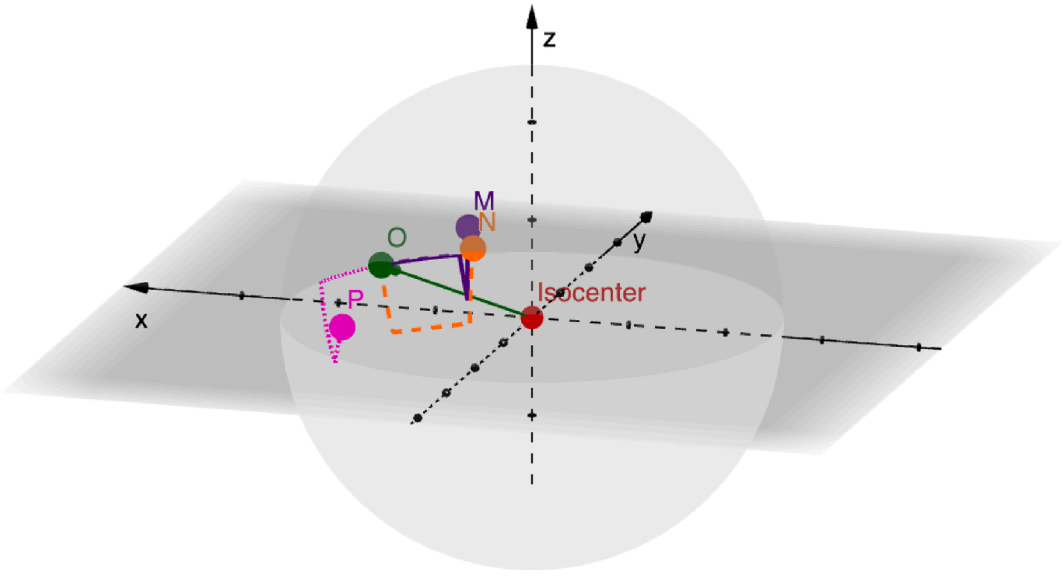

Fig. 1. Rotational order and direction effect. The object O located to 5 cm from the isocenter defined at the origin is rotated in the order: yaw, pitch, roll with an angle of 2° (solid lines). The final position is M. The object O is rotated in the order: pitch, yaw, roll with an angle of 2° (dashed lines). The final position is N. The object O is rotated in the order: yaw (−2°), pitch, roll with an angle of 2° (dotted lines). The final position is P.

the brainstem.

2.2. Institutional PTV margin criteria

The institutional PTV margin criteria followed is based on Kuntz et al. and others [7,14,23,24,46]. If the GTV is located less than 50 mm from the isocenter, a margin of 0.5 mm was assigned. If the GTV is located more than 50 mm from the isocenter or its volume was less than 0.1 cc, a margin of 1 mm was assigned.

2.3. Plan selection

Ten plans were selected. The average number of metastases was 5 ± 2 [3,9] per plan with an average GTV volume of 1.1 ± 1.3 cc [0.02, 5.1]. A total of 55 brain metastases were analyzed. The prescribed doses were 18, 21 and 25 Gy. Mean dose (D_{mean}) were 22.92 ± 1.03 Gy [22.02, 27.75], D_{95} were 20.65 ± 0.22 Gy [18.11, 24.69], D_{max} were 24.77 ± 1.28 Gy [23.25, 30.18] and Paddick conformity index (PCI) were 0.83 ± 0.04 Gy [0.66, 0.89]. Table 1 shows the plans as Brainlab Elements™ setup.

2.4. In-house software

A software was developed in MATLAB® version R2019b (MathWorks Inc., MA, USA), dedicated to rotate the structures of the plans. The software was performed following Dvorak's recommendations for handling radiotherapy DICOM files [47]. MATLAB® workflow is shown in Fig. 2. The software consists of four modules, for handling the CT (CT_{ijk}), dose (RD_{ijk}) and structure (RS_{ijk}) files, perform rotation for a given structure ($RS^{a'}_{ijk}$) and display dosimetric calculation. i,j,k are the number of rows, columns and slices of the matrices, respectively. The calculated DVH by MATLAB® was compared with the DVH of the TPS. Correspondence up to 3% was defined as validation criterion as reported by Dvorak [47].

The PCI and GI are calculated by MATLAB® based on the given dose matrix and structure and the formal definition of these indices [48–50]. The PCI is calculated as shown in equation (1):

$$PCI = \frac{TV_{PIV}^2}{TV \times PIV}. \quad (1)$$

where TV is the volume of the structure, $PIV$is the volume of the prescription isodose and TV_{PIV} is the volume of the structure covered by the prescription isodose. The PIV_{50} is the 50% volume of the prescription isodose. The GI is calculated as shown in Eq. (2):

$$GI = \frac{PIV_{50}}{PIV}. \quad (2)$$

The variation of the DVH was quantified from DVH degradation index ($DVHdi$) defined as the ratio of the DVH area of the displaced structure and the area of the original DVH, as shown in equation (3):

$$DVHdi = \frac{\int DVH'}{\int DVH} = \frac{\int_0^{D_{max}} V'\,dD}{\int_0^{Dmax} V dD}. \quad (3)$$

where V is the volume of the original structure, V' is the volume of the displaced structure, dD is the dose differential. This ratio must be close to unity to ensure that the objectives of the plan are covered even when the structure is displaced. The effect of degradation is shown in Fig. 3.

MATLAB® optimizes the maximum or minimum effective displacement generated by rotating in three directions (roll, pitch, yaw) through a GA based on elitism (which ensures global convergence). The dose

Table 1
Target (GTV) lesions defined according to the size and dosimetric parameters D_{95}, mean dose (D_{mean}), maximum dose (D_{max}), Paddick Conformity Index (PCI) reported by the treatment planning system (TPS) and their planning target (PTV) margin, target (GTV) volume and distance to isocenter.

Plan	D_{95} [Gy]	D_{mean} [Gy]	D_{max} [Gy]	PCI	PTV margin	Number of metastases	GTV volume [cc]	Distance to isocenter [mm]
1	20.70 [20.57, 20.79]	22.56 [22.10, 22.72]	24.36 [23.44, 24.73]	0.86 [0.84, 0.88]	0.5 mm	5	0.186 [0.101,0.312]	42 [37,47]
	20.68 [20.63, 20.74]	22.22 [22.02, 22.44]	23.66 [23.25, 24.19]	0.84 [0.82, 0.85]	1 mm	3	0.168 [0.077,0.327]	72 [55,89]
2	20.72	22.27	23.64	0.83	0.5 mm	1	0.514	44
	20.52 [20.41, 20.66]	22.82 [22.57, 23.24]	24.76 [24.29, 25.54]	0.85 [0.83, 0.88]	1 mm	4	1.069 [0.373,2.885]	55 [52,62]
3	20.53 [20.35, 20.70]	22.57 [22.29, 22.89]	24.38 [23.93, 25.01]	0.81 [0.79, 0.82]	0.5 mm	3	1.112 [0.117,2.147]	38 [33,41]
	20.60 [20.59, 20.60]	22.23 [22.22, 22.23]	23.62 [23.52, 23.71]	0.81 [0.77, 0.85]	1 mm	2	0.172 [0.159,0.186]	66 [60,72]
4	20.84	22.48	23.91	0.84	0.5 mm	1	0.397	21
	20.81 [18.11, 24.69]	24.14 [22.33, 25.47]	27.14 [24.05, 30.18]	0.76 [0.66, 0.85]	1 mm	5	0.769 [0.020,3.605]	48 [28,75]
5	20.59	22.81	24.56	0.85	0.5 mm	1	1.236	41
	20.44	22.50 [22,48,22,52]	24.00 [23.85, 24.14]	0.84 [0.83, 0.85]	1 mm	2	3.569 [2.066,5.072]	62 [58,65]
6	20.43	23.11	25.55	0.88	0.5 mm	1	0.638	27
	20.56 [20.50, 20.62]	22.41 [22.26, 22.56]	23.90 [23.55, 24.24]	0.85 [0.81, 0.89]	1 mm	2	3.022 [1.014,5.031]	62 [59,65]
7	20.60	22.98	25.01	0.85	0.5 mm	1	0.911	35
	20.68 [20.48, 20.80]	22.33 [22.05, 22.70]	23.91 [23.36, 24.55]	0.85 [0.83, 0.88]	1 mm	3	0.532 [0.069,1.452]	40 [14,59]
8	20.64 [20.47, 20.77]	22.54 [22.40, 22.65]	24.32 [24.00, 24.68]	0.82 [0.78, 0.88]	0.5 mm	3	1.221 [0.224,2.421]	36 [24,47]
	20.56	22.39	23.82	0.84	1 mm	1	0.89	52
9	20.60 [20.42, 20.79]	22.80 [22.34, 23.60]	24.85 [24.08, 25.73]	0.81 [0.76, 0.85]	0.5 mm	4	0.847 [0.165,2.297]	36 [26,44]
	20.94 [20.62, 21.23]	24.04 [23.46, 24.63]	26.89 [26.15, 27.75]	0.77 [0.69, 0.84]	1 mm	4	0.049 [0.029,0.069]	56 [32,101]
10	20.62 [20.52, 23.25]	22.70 [22.24, 23.25]	24.64 [23.67, 25.81]	0.84 [0.75, 0.88]	0.5 mm	5	0.706 [0.123,2.275]	47 [43,50]
	20.65 [20.58, 20.78]	22.78 [22.63, 22.92]	24.76 [24.37, 25.08]	0.86 [0.83, 0.89]	1 mm	4	0.219 [0.031,0.416]	66[53,75]

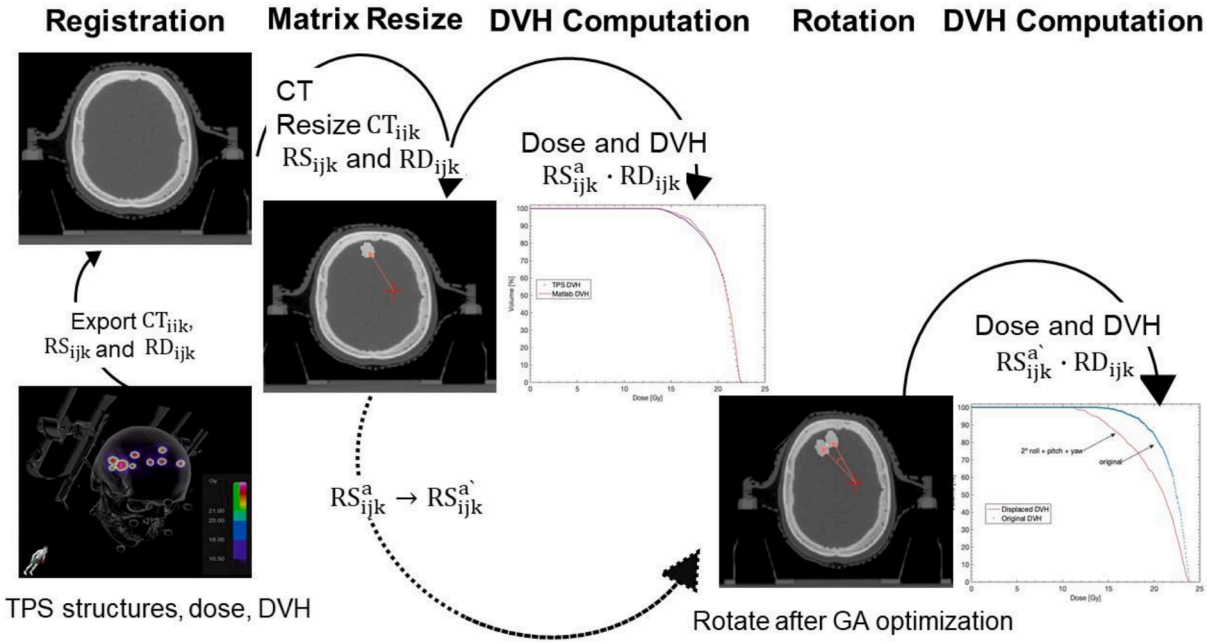

Fig. 2. MATLAB® workflow. The software handles the computed tomography CT (CT_{ijk}), dose (RD_{ijk}), and structure (RS_{ijk}), files. The treatment planning system (TPS) RD_{ijk}, plan, dose-volume histogram (DVH), structure (a) and CT_{ijk} are exported and registered to MATLAB. MATLAB® resizes the CT_{ijk} and RD_{ijk} matrix and compares the TPS DVH and the computed DVH for the structure a. By the use of genetic algorithm (GA) to optimize the displacement produced for rotations, the structure a is rotated. DVH is re-calculated for the rotated structure a' and compared with the original DVH.

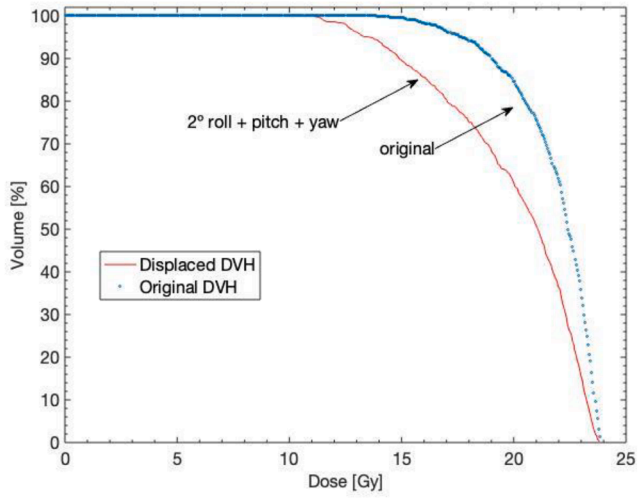

Fig. 3. Dose-Volume Histogram (DVH) degradation effect produced by displacements in the target volume due to 2° rotations in three directions (roll, pitch and yaw).

matrix is maintained fixed while the GTV is displaced applying a given rotational combination encoded by binary elements as shown in Fig. 2. The effective displacement is calculated as the module of the difference vector $|\widehat{r}_{oo'}| = |\widehat{r}_{oi} - \widehat{r}_{o'i}|$ where o is the center of mass of the original structure, o' is the center of mass of the displaced structure, i is the isocenter defined in the coordinate system of the CT image set.

2.5. Genetic algorithm

GA was implemented using an initial artificial population of 4 encoded solutions (chromosomes) composed by 6 binary elements (genes) of the form $x_i = \in_{ij}$ where i is the i-th chromosome, j represents the genes of each chromosome. The point on the chromosome that is defined by j is known as allele.

2.5.1. GA structure

1. Chromosome encoding: The first allele is defined for $j \leq 3$. Elements $\in_{ij}$ were transformed from the binary to the decimal system. There were 8 combinations in total for the first allele and each one was assigned a particular combination of the order in which the couch rotations were performed. The second allele is defined for $j \geq 4$. Elements $\in_{ij}$ correspond to the rotational direction. If the gene $\in_{ij}$is 1, the direction is clockwise (CW). Otherwise, it is counterclockwise (CCW). Next, a chromosome is represented in Fig. 4.

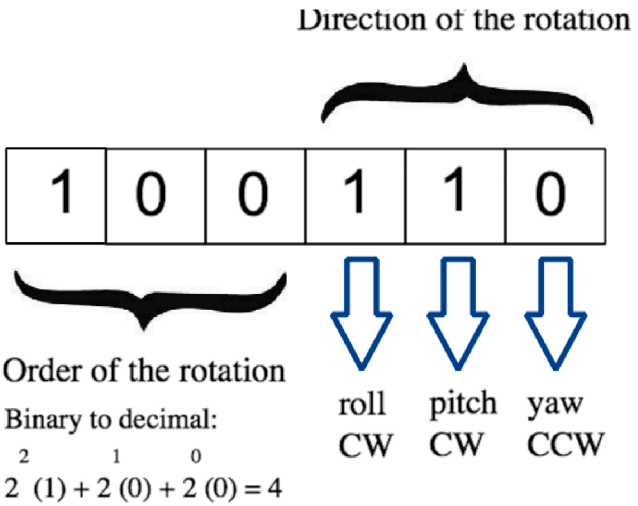

Fig. 4. Generated chromosome structure. The first three genes correspond to the rotational order. Each combination is encoded from binary to decimal, and each decimal number between 1 and 8 is associated with a specific rotation order. The last three genes correspond to the rotational direction: clockwise (CW) or counterclockwise (CCW).

2. Fitness: The fitness function corresponded to the maximum effective displacement between the centers of mass of the volume of the original and rotated targets.
3. Selection: From each generation, the two chromosomes that had the best fitness were selected. The method used was selection of survivors using elitism (to ensure global convergence).
4. Recombination: The uniform probability function was used to determine the crossover point by diagonal crossing and to determine if the $\in_{ij}$ gene was mutated.
5. Evolution: The number of generations was optimized. From the targets studied, the variation of the maximum displacement of the best chromosome of generation k and of the final generation for rotations with small angles ($\theta \leq 2$) was analyzed. The displacement of each generation was calculated. The variation with respect to the global maximum displacement was calculated with respect to the number of generations of the GA.

2.6. Displacements

The maximum and minimum displacements for the GTV were obtained through GA. 0.5°, 1° and 2° in yaw, pitch, roll, were used to carry out the optimization. The variations of D_{mean}, D_{99}, PCI and GI were obtained from the displaced targets.

2.7. PTV optimized margin

An optimization of the PTV margin is proposed as a function of the maximum displacement determined by the GA. Given a rotation of 0.5°, 1° or 2° in all directions, the maximum displacement defined the margin that was given to PTV. Following this optimized criterion, the plans were recalculated in the TPS, assigning margins of 0.5, 1, 1.5 or 2 mm as appropriate for the GTV. Optimized plans were exported to MATLAB®. Dosimetric parameters applying the same rotational combination displacements as in the adopted PTV margin criterion for the GTVs were re-evaluated in MATLAB®. The new GTV dosimetric variations due to rotations in these plans were compared to the equivalent dosimetric variations to the plans following the institutional protocol (0.5 mm or 1 mm).

3. Results

The MATLAB® and TPS calculated DVHs are shown in Fig. 5. Correspondence up to 1% was obtained, fulfilling Dvorak's criteria for DVH equivalence [42].

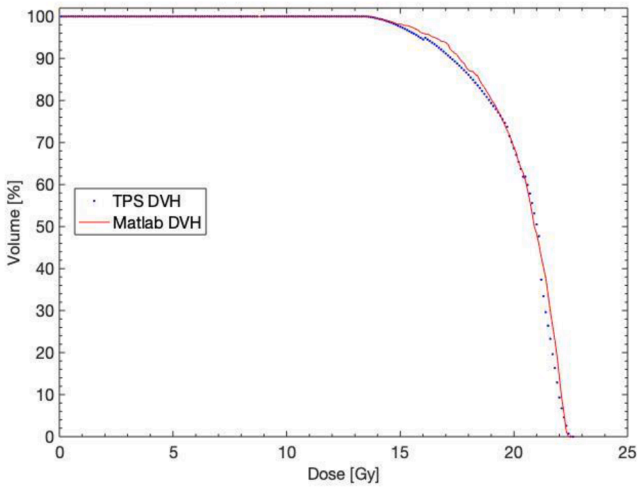

Fig. 5. Comparison of the original Dose-Volume Histogram (DVH) of the treatment planning system (TPS) and that obtained by MATLAB®.

The effective displacements for the 48 possible combinations as an example of 2° rotations in the three directions applied to a GTV at 52 mm from the isocenter are shown in Table 2. It was determined that with 8 generations there was global convergence. The behavior of the optimization as a function of the number of generations is presented in Fig. 6.

The maximum and minimum displacements for the GTV are shown in Fig. 7. As expected, the maximum displacements were longer (up to 4 mm) for targets located beyond 50 mm from the isocenter than targets located near to the isocenter (up to 2.5 mm). There were statistically significant differences using Student's t-test between the maximum and minimum displacements ($p < 9 \times 10^{-8}$ for both intervals).

The displacements up to 0.5 mm differences were 1% for D_{mean} and less than 13% for D_{99}, CPI and GI. This implied that with the PTV margin convention adopted, it was possible to reduce the dosimetric detriment in the GTV significantly to less than 13% with the established margins. For displacements up to 1 mm the differences of 10% for D_{mean}, 28% for D_{99} and less than 50% for CPI and GI as shown in Figs. 8–11.

The dosimetric detriment of *DVHdi* as a function of the effective displacement is shown in Fig. 12. For displacements shorter than 1 mm, the degradation of DVH reached down to 95%. For longer displacements, the degradation of the DVH was evident (down to 34% for 4 mm). Consideration of this index is recommended to complement the dosimetric analysis of a SIMM-SRS plan.

The differences between the institutional and optimized criteria for PTV were statistically significant regarding the differences in variations of the GTV for D_{mean} ($p = 0.02$), D_{99} ($p = 0.04$), PCI ($p = 0.02$) and GI ($p = 0.02$) due to rotations. The differences between the two PTV margin criteria are shown in Fig. 13. Optimized margins avoid the detriment of dosimetric parameters as shown in this work to consider the dosimetric differences for the adopted and optimized PTV margins. The differences were reduced for D_{mean} (from $2 \pm 2\%$ to $1 \pm 1\%$), D_{99} (from $8 \pm 9\%$ to $4 \pm 1\%$), PCI (from $-35 \pm 51\%$ to $-12 \pm 16\%$) and GI (from $-3 \pm 6\%$ to $-0.5 \pm 6\%$). Greater margins, considering the adopted and optimized PTV margins were associated with an increase in V_{12} (from $15 \pm 9\%$ to $18 \pm 6\%$) and V_{10} (from $21 \pm 6\%$ to $25 \pm 8\%$) in the healthy brain, as shown in Table 3. The mean values and standard deviations are presented in Table 3.

In addition, Fig. 14 shows the differences in the PTV volumes and the volumes that received 12, 10 and 5 Gy (V_{12}, V_{10} and V_5, respectively) in

Table 2
Displacements obtained by the 48 possible combinations of a target (GTV) located 52 mm from the isocenter. Rotations were roll (R), pitch (P) and yaw (Y). The direction was clockwise (CW) or counterclockwise (CCW).

Rotational combination	Displacement [mm]
R-CCW Y-CCW P-CCW, Y-CCW R-CCW P-CCW, R-CCW Y-CCW P-CW, YCCW R-CCW P-CW	0.2
R-CW Y-CCW P-CCW, Y-CCW R-CW P-CCW	0.4
R-CW Y-CCW P-CW, Y-CCW R-CW P-CW	0.5
R-CCW Y-CW P-CW, Y-CW R-CCW P-CW,R-CCW Y-CW P-CCW, Y-CW R-CCW P-CCW	0.6
R-CW Y-CW P-CCW, Y-CW R-CW P-CCW	0.7
R-CW Y-CW P-CW, Y-CW R-CW P-CW	0.8
P-CW Y-CW R-CW, Y-CW P-CW R-CW, P-CCW Y-CW R-CW, Y-CW P-CCW R-CW, P-CW Y-CW R-CCW, Y-CW P-CW R-CCW, P-CCW Y-CW R-CCW, Y-CW P-CCW R-CCW	1.8
P-CW Y-CCW R-CW, Y-CCW P-CW R-CW, P-CCW Y-CCW R-CCW, Y-CCW P-CCW R-CCW, P-CW Y-CCW R-CCW, Y-CCW P-CW R-CCW, P-CCW Y-CCW R-CW, Y-CCW P-CCW R-CW	1.9
P-CCW R-CW Y-CW	2.8
R-CW P-CW Y-CW, P-CW R-CW Y-CW, R-CW P-CW Y-CCW, R-CW P-CCW Y-CW, R-CCW P-CW Y-CW, P-CW R-CCW Y-CW, R-CCW P-CCW Y-CW, P-CCW R-CCW Y-CW	2.9
R-CCW P-CCW Y-CCW, P-CCW R-CCW Y-CCW, R-CCW P-CW Y-CCW, P-CW R-CCW Y-CCW, R-CW P-CCW Y-CCW, P-CCW R-CW Y-CCW	3.0

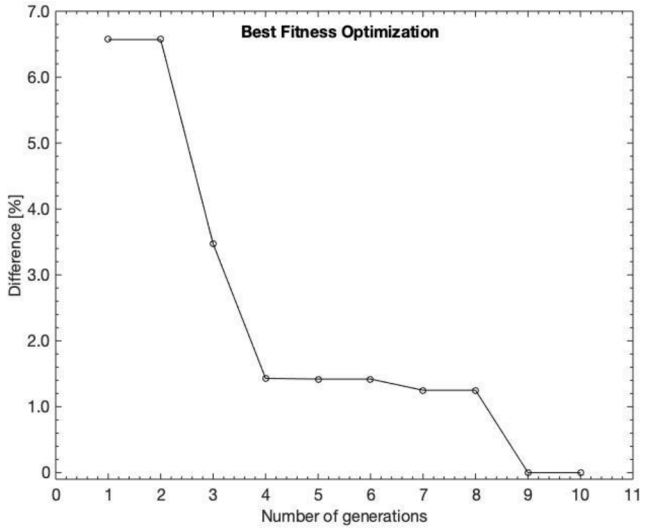

Fig. 6. The fitness function (longest effective displacement) differences for each chromosome population was obtained up to 10 generations. The difference between the optimized fitness for each generation and the global fitness is represented as a function of the number of generations.

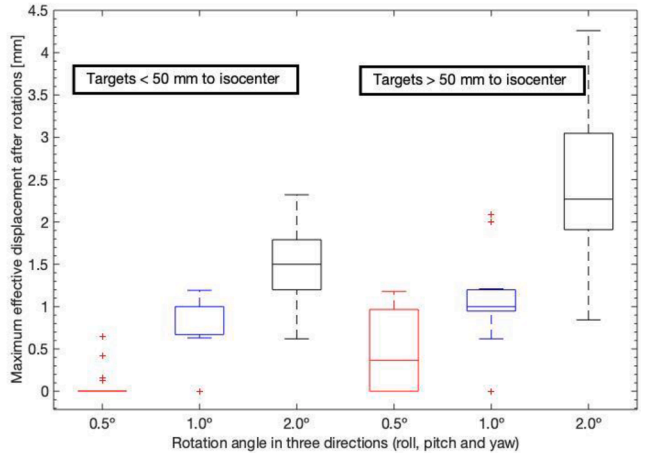

Fig. 7. Maximum effective displacements obtained after rotating 0.5°, 1° and 2° in the three directions for targets located shorter than 50 mm from the isocenter and beyond 50 mm from the isocenter.

the healthy brain between the plans with the adopted margin convention and the margin-optimized plans. The mean values and standard deviations of V_{12}, V_{10} and V_5 are presented in Table 4. The differences determined for both groups of plans of these dosimetric parameters are statistically significant ($p < 0.02$).

4. Discussion

The order and direction in which the rotations are applied with respect to the isocenter affect the final position in which GTV is located. For GTV located at a distance less than 50 mm from the isocenter, it is possible to calculate a maximum effective displacement of 2.5 mm. By means of a classical GA, it is possible to attain this value without performing the calculations for all possible combinations of the rotational order. For GTV beyond 50 mm from the isocenter, the displacement was up to 4 mm. It is noticeable that even small rotation angles of 0.5° were translated into displacements greater than the tolerances allowed with the use of image-guided systems in SRS treatment of multiple metastases where tolerances are 0.5°/0.5 mm. This fact shows that it is

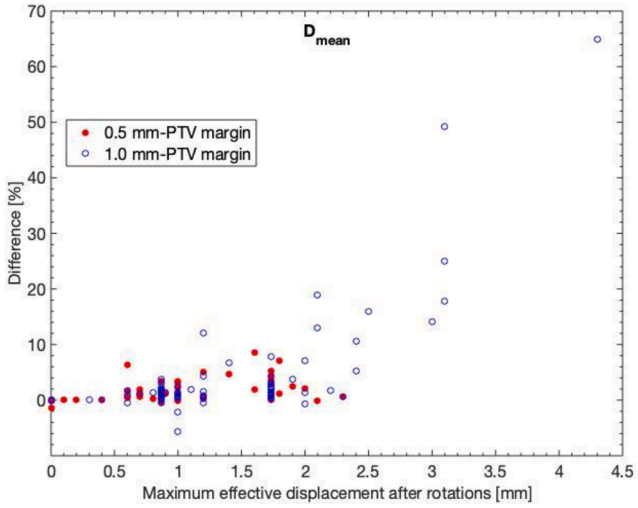

Fig. 8. Difference of mean dose (D_{mean}) for the target (GTV) displaced as a function of the maximum effective displacement.

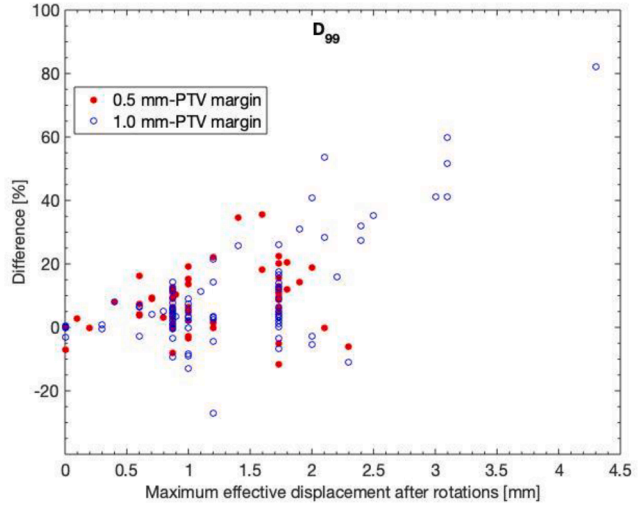

Fig. 9. Difference of D_{99} for the GTV displaced as a function of the maximum effective displacement.

indispensable to use a robotic table in SIMM-SRS plans.

The optimization of the PTV margin had remarkable improvement in the dosimetric variations of the plans as presented in Fig. 13. The use of margins in SIMM-SRS plans, based on geometric expansion criteria [8], does not take into account the uncertainties generated by the position of each target in relation to the isocenter, nor the direction and order of the rotations. The use of fixed values of GTV-to-PTV extension by the distance between the center of mass of the GTV and the isocenter criterion may be insufficient depending on the location of each target with respect to the isocenter. At the present time, the treatment planning systems generate PTV margins from boolean mathematical operations. Based on the results of this work it is shown that these margins may be dependent on the distance to the isocenter. The development of adaptive margins in function of their relative position to the isocenter and dosimetric parameters is proposed as future work.

The determination of the PTV margin entailed greater GTV dose coverage considering the setup uncertainties due to rotations. However, the optimization of the margins given to the PTV led to an increase in the volume of irradiated healthy brain. The increase in V_{12} and V_{10} in the healthy brain is associated with a greater risk of necrosis [51–53].

In this study we were focused on the effect of rotations. The

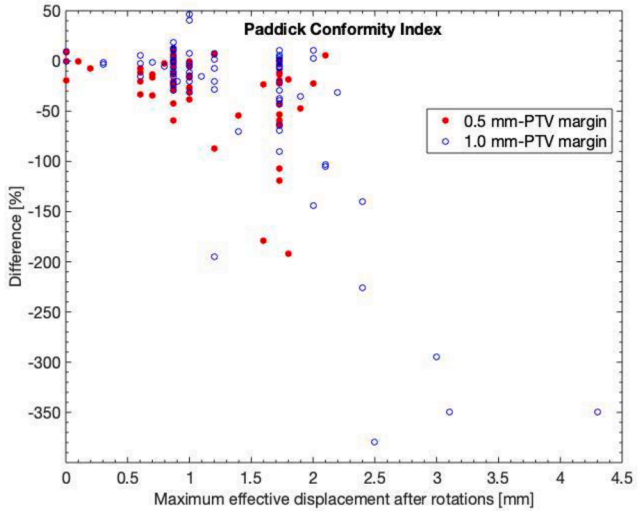

Fig. 10. Difference of Paddick Conformity Index (PCI) for the target (GTV) displaced as a function of the maximum effective displacement.

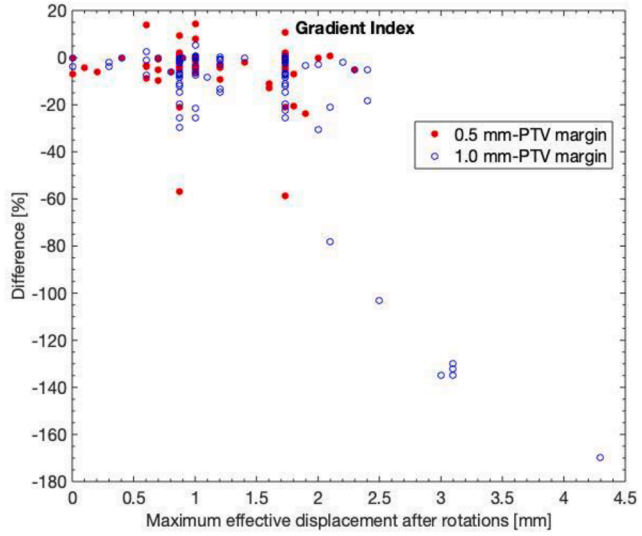

Fig. 11. Difference of Gradient Index (GI) for the target (GTV) displaced as a function of the maximum effective displacement.

combined effect of translations and rotations was not considered. This combination could generate greater displacements and their dosimetric impact will be studied later. Given the encoded structure of the chromosomes in the GA, it is possible to include information associated with translational displacements, dosimetric and medical parameters that allow to optimize the PTV margins based on geometric, dosimetric and medical information.

5. Conclusion

The order and direction of the rotations directly influence the final uncertainties position of the GTV location in a SIMM-SRS. Different rotational combinations do not lead to the same displaced point. It is necessary to take into account the maximum possible displacement to endure, it is appropriate to optimize taking into account this displacement and it is convenient to optimize the calculation process to arrive to such value. Some lesions, due to its relative position to isocenter, were shown to be more sensitive to rotation errors with regarding to the dosimetric consequences.

It is possible to optimize the margin that must be assigned to the PTV

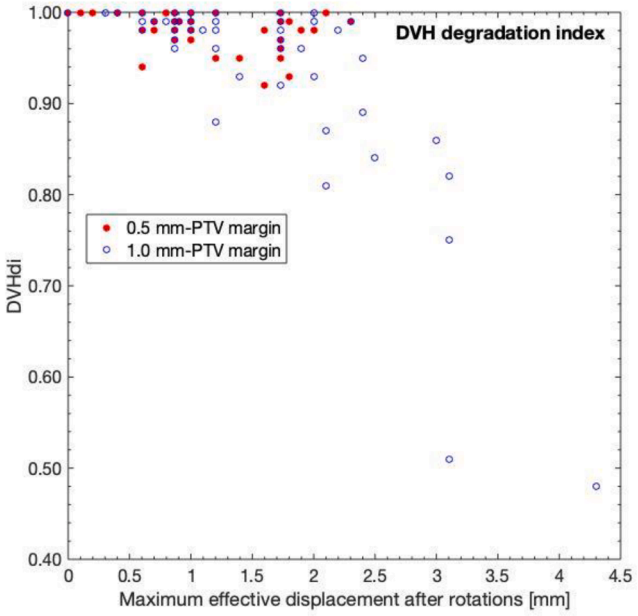

Fig. 12. Dose-Volume Histogram (DVH) degradation index (DVHdi) is represented as the DVH area ratio between the displaced and the original structures. The DVHdi as a function of the maximum effective displacement for each target is represented. It is shown the remarkable dosimetric detriment for displacements beyond 1 mm.

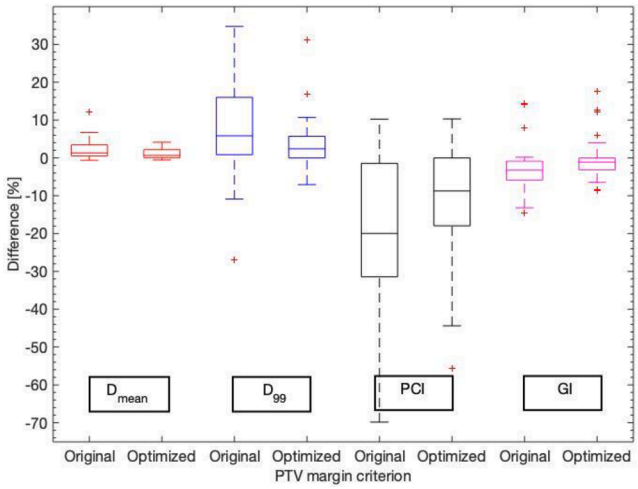

Fig. 13. Comparison of the dosimetric differences for mean dose (D_{mean}), D_{99}, Paddick conformity index (PCI) and gradient index (GI) between the plans with the planning target volume (PTV) adopted convention (original) and the margin-optimized (optimized) plans based on the genetic algorithm (GA).

Table 3
Mean values and standard deviations for mean dose (D_{mean}), D_{99}, Paddick conformity index (PCI) and gradient index (GI) differences for the planning target volume (PTV) margins following the criteria adopted (0.5 mm- or 1 mm-PTV margin) and the margin optimized by the genetic algorithm (GA). The p-values are shown.

	Adopted margin criterion (0.5/1 mm) [%]	Optimized-margin PTV [%]	p
D_{mean}	2 ± 2	1 ± 1	0.02
D_{99}	8 ± 9	4 ± 1	0.04
PCI	−35 ± 51	−12 ± 16	0.02
GI	−3 ± 6	−0.5 ± 6	0.02

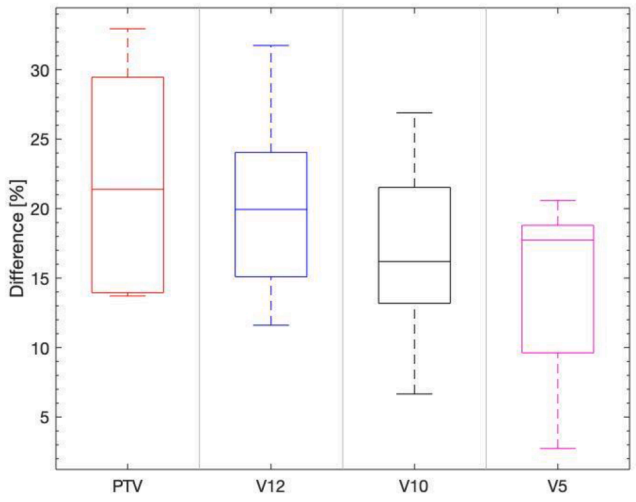

Fig. 14. The volumes that received 12, 10 and 5 Gy (V_{12}, V_{10} and V_5, respectively) of healthy brain and PTV volumes differences between the plans followed with the adopted convention and the plans optimized through the genetic algorithm.

Table 4
Mean values and standard deviations for planning target volume (PTV), the volumes that received 12, 10 and 5 Gy (V_{12}, V_{10} and V_5, respectively) of healthy brain differences in the plans following the criteria adopted and the margin optimized by the genetic algorithm (GA). The p-values are shown.

	Adopted margin criterion (0.5/1 mm) [cc]	Optimized-margin PTV [cc]	p
PTV volume	8 ± 3	10 ± 4	–
V_{12}	15 ± 9	18 ± 6	0.02
V_{10}	21 ± 6	25 ± 8	0.03
V_5	73 ± 25	83 ± 26	0.02

based on the GTV maximum calculated displacement. The proposed GA allows to obtain the GTV maximum displacement in a less time-consuming way. Optimized PTV margins reduce the detriment of dosimetric parameters. Greater PTV margins are associated with an increase in healthy brain volume, which could increase the risk of necrosis. The use of margins in SIMM-SRS, based solely on geometric expansion criteria, does not take into account the uncertainties generated by the position of each target in relation to the isocenter, nor the direction and order of the rotations. The use of fixed GTV-to-PTV extension values with respect to the distance from the center of mass to the isocenter may be insufficient depending on the location of each target with respect to the isocenter.

The use of GA offers a novel tool to obtain information concerning to the maximum displacement performed by the order and the direction of rotations. The use of the optimized PTV margins increases the dose in healthy brain and OARs. It is decision of the radiation oncologist to admit values above than the accepted for probability of necrosis. This work is a mathematical, geometric and dosimetric study of the impact that the rotational order has on SIMM-SRS treatments. The inclusion of site-specific medical considerations is necessary.

References

[1] Bilger A, Frenzel F, Oehike O, Wiehle R, Milanovic D, Prokic V, et al. Local control and overall survival after frameless radiosurgery: a single center experience. Clin Transl Radiat Oncol. 2017;7:55–61. https://doi.org/10.1016/j.ctro.2017.09.007.
[2] Karlsson B, Hanssens P, Wolff R, Söderman M, Lindquist C, Beute G. Thirty years' experience with Gamma Knife surgery for metastases to the brain. J Neurosurgery 2009;111:449–57. https://doi.org/10.3171/2008.10.JNS08214.
[3] Nichol A, Ma R, Hsu F, Gondara L, Carolan H, Olson R, et al. Volumetric radiosurgery for 1 to 10 brain metastases: a multicenter, single-arm, phase 2 study. Int J Radiat Oncol Biol Phys. 2016;94:312–21. https://doi.org/10.1016/j.ijrobp.2015.10.017.
[4] Yamamoto M, Serizawa T, Shuto T, Akabane A, Higuchi Y, Kawagishi J, et al. Stereotactic radiosurgery for patients with multiple brain metastases (JLGK0901): a multi-institutional prospective observational study. Lancet Oncol 2014;15:43–9. https://doi.org/10.1016/S1470-2045(14)70061-0.
[5] Izard M, Moutrie V, Rogers J, Beath K, Grace M, Karle B, et al. Volume not number of metastases: Gamma Knife radiosurgery management of intracranial lesions from an Australian perspective. Radiother Oncol 2019;133:43–9. https://doi.org/10.1016/j.radonc.2018.12.018.
[6] Nikitas J, Roach M, Robinson C, Bradley J, Huang J, Perkins S, et al. Treatment of oligometastatic lung cancer with brain metastases using stereotactic radiosurgery (SRS) and stereotactic body radiation therapy (SBRT). Clin Transl Radiat Oncol. 2020;21:32–5. https://doi.org/10.1016/j.ctro.2019.12.001.
[7] Kuntz L, Matthis R, Wegner N, Lutz S. Dosimetric comparison of mono-isocentric and multi-isocentric plans for oligobrain metastases: A single institutional experience. Cancer Radiother 2020;24–1:53–9. https://doi.org/10.1016/j.canrad.2019.10.003.
[8] Stanhope C, Chang Z, Wang Z, Yin F, Kim G, Salama JK, et al. Physics considerations for single-isocenter, volumetric modulated arc radiosurgery for treatment of multiple intracranial targets. Pract Radiat Oncol. 2016;6–3:207–13. https://doi.org/10.1016/j.prro.2015.10.010.
[9] Usui K, Isobe A, Hara N, Muroi T, Sajiki O, Ogawa K, et al. Development of a rotational set-up correction device for stereotactic head radiation therapy: a performance evaluation. J Appl Clin Med Phys. 2019;20–6. https://doi.org/10.1002/acm2.12616.
[10] Winey B, Bussiére M. Geometric and dosimetric uncertainties in intracranial stereotactic treatments for multiple nonisocentric lesions. J Appl Clin Med Phys. 2014;15–3:122–32. https://doi.org/10.1120/jacmp.v15i3.4668.
[11] Ruggieri R, Naccarato S, Mazzola R, Ricchetti F, Corradini S, Fiorentino A, et al. Linac-based VMAT radiosurgery for multiple brain lesions: comparison between a conventional multi-isocenter approach and a new dedicated mono-isocenter technique. Radiat Oncol. 2018;13:38. https://doi.org/10.1186/s13014-018-0985-2.
[12] Li G, Ballangrud A, Chan M, Ma R, Beal K, Yamada Y, et al. Clinical experience with two frameless stereotactic radiosurgery (fSRS) systems using optical surface imaging for motion monitoring. J Appl Clin Med Phys. 2015;16:149–62. https://doi.org/10.1120/jacmp.v16i4.5416.
[13] Dhabaan A, Schreibmann E, Siddigi A, Elder E, Fox T, Ogunleye T, et al. Six degrees of freedom CBCT-based positioning for intracranial targets treated with frameless stereotactic radiosurgery. J Appl Clin Med Phys 2012;13–6:215–25. https://doi.org/10.1120/jacmp.v13i6.3916.
[14] Ezzell GA. The spatial accuracy of two frameless, linear accelerator-based systems for single-isocenter, multitarget cranial radiosurgery. J Appl Clin Med Phys. 2017;18:37–43. https://doi.org/10.1002/acm2.12044.
[15] Zhang M, Zhang Q, Gan H, Li S, Zhou S. Setup uncertainties in linear accelerator based stereotactic radiosurgery and a derivation of the corresponding setup margin for treatment planning. Phys Med. 2016;32–2:379–85. https://doi.org/10.1016/j.ejmp.2016.02.002.
[16] Selvan KT, Padma G, Revathy MK, Raj N, Senthilnathan K, Babu PR. Dosimetric effect of rotational setup errors in single-isocenter volumetric-modulated arc therapy of multiple brain metastases. J Med Phys. 2019;44–2:84–90. https://doi.org/10.4103/jmp.JMP_103_18.
[17] Kang KM, Chai GY, Jeong BK. Estimation of optimal margin for intrafraction movements during frameless brain radiosurgery. Med Phys. 2013;40:051716. https://doi.org/10.1118/1.4801912.
[18] Sagawa T, Ohira S, Ueda Y, Akino Y, Mizuno H, Matsumoto M, et al. Dosimetric effect of rotational setup errors in stereotactic radiosurgery with HyperArc for single and multiple brain metastases. J Appl Clin Med Phys. 2019;20:84–91. https://doi.org/10.1002/acm2.12716.
[19] Keeling V, Hossain S, Jin H, Algan O, Ahmad S, Ali I. Quantitative evaluation of patient setup uncertainty of stereotactic radiotherapy with the frameless 6D ExacTrac system using statistical modeling. J Appl Med Phys. 2016;17–3:111–27. https://doi.org/10.1120/jacmp.v17i3.5959.
[20] Hosang J, Keeling V, Ali I, Ahmad S. Dosimetric effects of positioning shifts using 6D-frameless stereotactic Brainlab system in hypofractionated intracranial radiotherapy. J Appl Clin Med Phys. 2016;17:102–11. https://doi.org/10.1120/jacmp.v17i1.5682.
[21] Kirkpatrick JP, Wang Z, Sampson JH, McSherry F, Herndon JE, Allen KJ, et al. Defining the optimal planning target volume in image-guided stereotactic radiosurgery of brain metastases: results of a randomized trial. Int J Radiat Oncol Biol Phys. 2015;91–1:100–8. https://doi.org/10.1016/j.ijrobp.2014.09.004.
[22] Mori Y, Kaneda N, Hagiwara M, Ishiguchi T. Dosimetric study of automatic brain metastases planning in comparison with conventional multi-isocenter dynamic conformal arc therapy and gamma knife radiosurgery for multiple brain metastases. Cureus 2016;8–11:e882. https://doi.org/10.7759/cureus.882.
[23] Guckenberger M, Roesch J, Baier K, Sweenwy RA, Flentje M. Dosimetric consequences of translational and rotational errors in frame-less image-guided radiosurgery. Radiat Oncol. 2012;63–7. https://doi.org/10.1186/1748-717X-7-63.
[24] Jhaveri J, Chowdhary M, Zhang X, Press RH, Switchenko JM, Ferris MJ, et al. Does size matter? Investigating the optimal planning target volume margin for postoperative stereotactic radiosurgery to resected brain metastases. J Neurosurg. 2018;130–3:797–803. https://doi.org/10.3171/2017.9.JNS171735.

[25] Roper J, Chanyavanich V, Betzel G, Switchenko J, Dhabaan A. Single-isocenter multiple-target SRS: risk of compromised coverage. Int J Radiat Oncol. Biol. Phys. 2015. https://doi.org/10.1016/j.ijrobp.2015.07.2262.
[26] Liu RJ, Yang SX, Neylon J, Hall MD, Dandaoani S, Vora N, et al. Residual setup errors in cranial stereotactic radiosurgery without six degree of freedom robotic couch: frameless versus rigid immobilization systems. J Appl Clin Med Phys. 2020; 21:87–93. https://doi.org/10.1002/acm2.12828.
[27] Clark GM, Fiveash JB, Prendergast BM, Willey CW, Spencer SA, Thomas EM, et al. Dosimetric impact of patient rotational setup errors with frameless single-isocenter, multi-target volumetric modulated arc radiosurgery for multiple brain metastases. Int J Radiat Oncol Biol Phys. 2011;81–2:S888.
[28] Chang J. A statistical model for analyzing the rotational error of single isocenter for multiple targets technique. Med Phys. 2017;44–6:2115–23. https://doi.org/10.1002/mp.12262.
[29] Nakano H, Tanabe S, Utsunomiya S, Yamada T, Sasamoto R, Nakano T, et al. Effect of setup error in the single-isocenter technique on stereotactic radiosurgery for multiple brain metastases. J Appl Clin Med Phys. 2020;21–12:155–65. https://doi.org/10.1002/acm2.13081.
[30] Kim S, Jin H, Yang H, Amdur RJ. A study on target positioning error and its impact on dose variation in image-guided stereotactic body radiotherapy for the spine. Int J Radiat Oncol Biol Phys. 2009;73–5:P1574–9. https://doi.org/10.1016/j.ijrobp.2008.12.023.
[31] Gevaert T, Verellen D, Engels B, Depuydt T, Heunickx K, Tournel K, et al. Clinical evaluation of a robotic 6-degree of freedom treatment couch for frameless radiosurgery. Int J Radiat Oncol Biol Phys. 2015;16–5:35–45. https://doi.org/10.1120/jacmp.v16i5.5525.
[32] Murphy MJ. Image-guided patient positioning: if one cannot correct for rotational offsets in external-beam radiotherapy setup, how should rotational offsets be managed? Med Phys. 2007;34:1880–3. https://doi.org/10.1118/1.2731485.
[33] McCall J. Genetic algorithms for modelling and optimization. J Comput Appl Math 2005;184–1:205–22. https://doi.org/10.1016/j.cam.2004.07.034.
[34] Engelbrecht AP. Computational Intelligence: An Introduction. (2nd ed.). Wiley Publishing; 2007.
[35] Reddy GT, Reddy MPK, Lakshmanna K, Rajput DS, Srivastava G. Hybrid genetic algorithm and a fuzzy logic classifier for heart disease diagnosis. Evol Intel 2020; 13:185–96. https://doi.org/10.1007/s12065-019-00327-1.
[36] Zhi H, Liu S. Face recognition based on genetic algorithm. J Vis Commun Image Represent 2019;58:495–502. https://doi.org/10.1016/j.jvcir.2018.12.012.
[37] Hanh NT, Binh HTT, Hoai NX, Palaniswami MS. An efficient genetic algorithm for maximizing area coverage in wireless sensor networks. 488(2019): 58-75. DOI: 10.1016/j.ins.2019.02.059.
[38] Pan X, Zhang T, Yang Q, Yang D, Rwigema JC, Qi XS. Survival prediction for oral tongue cancer patients via probabilistic genetic algorithm optimized neural network models. British Institute of Radiology. 93(2020):1112. Doi: 10.1259/bjr.20190825.
[39] Medical Physics. Institute of Radiooncology, KFJ Hospital Vienna. Dosimetric Parameters of the HD120 MLC. https://www.wienkav.at/kav/kfj/91033454/physik/tb/tb_hd120.htm. Accessed October 6, 2020.
[40] Lo SS, et al. Stereotactic body radiation therapy, medical radiology. In: Radiation Oncology. Berlin Heidelberg: Springer-Verlag; 2012. https://doi.org/10.1007/174_2012_635.
[41] Vergalasova I, Liu H, Alonso-Basanta M, Dong L, Li J, Nie K, et al. Multi-Institutional Dosimetric Evaluation of Modern Day Stereotactic Radiosurgery (SRS) Treatment Options for Multiple Brain Metastases. Front. Oncol. 9(2019):483. Doi: 10.3389/fonc.2019.00483.
[42] Gevaert T, Steenbeke F, Pellegri L, Engels B, Christian N, Hoornaert MT, et al. Evaluation of a dedicated brain metastases treatment planning optimization for radiosurgery: a new treatment paradigm? Radiat Oncol. 2016;11–13. https://doi.org/10.1186/s13014-016-0593-y.
[43] Mohan R, Chui C, Lidofsky L. Energy and angular distributions of photons from medical linear accelerators. Med Phys. 1985;12–5:592–7. https://doi.org/10.1118/1.595680.
[44] Mohan R, Chui C, Lidofsky L. Differential pencil beam dose computation model for photons. Med Phys. 1986;13–1:64–73. https://doi.org/10.1118/1.595924.
[45] Mohan R, Chui CS. Use of fast Fourier transforms in calculating dose distributions for irregularly shaped fields for three-dimensional treatment planning. Med Phys. 1987;14–1:70–7. https://doi.org/10.1118/1.596097.
[46] Novalis Circle Symposium. Impact of margins for single isocenter multiple target treatments AAPM 2019. https://www.novaliscircle.org/video/impact-of-margins-for-single-isocenter-multiple-target-treatments-dWQSM9a/. Accessed October 8, 2020.
[47] Dvorak P. Clinical Radiotherapy Physics with MATLAB: A Problem-Solving Approach. (1st edition). CRC Press; 2018.
[48] Paddick I, Lippitz B. A simple dose gradient measurement tool to complement the conformity index. J Neurosurg (Suppl) 2006;105:194–201. https://doi.org/10.3171/sup.2006.105.7.194.
[49] Balagamwala EH, Suh JH, Barnett GH, Khan MK, Neyman G, Cai RS, et al. The importance of the conformality, heterogeneity, and gradient indices in evaluating gamma knife radiosurgery treatment plans for intracranial meningiomas. Int J Radiat Oncol Biol Phys. 2012;83–1:1406–13. https://doi.org/10.1016/j.ijrobp.2011.10.024.
[50] Wagner TH, Bova FJ, Friedman WA, Buatti JM, Bouchet LG, Meeks SL. A simple and reliable index for scoring rival stereotactic radiosurgery plans. Int J Radiat Oncol Biol Phys. 2003;57–4:1141–9. https://doi.org/10.1016/s0360-3016(03)01563-3.
[51] Blonigen BJ, Steinmetz RD, Levin L, Lamba MA, Warnick RE, Breneman JC. Irradiated volume as a predictor of brain radionecrosis after linear accelerator stereotactic radiosurgery. Int J Radiat Oncol Biol Phys 2010;77–4:996–1001. https://doi.org/10.1016/j.ijrobp.2009.06.006.
[52] Flickinger JC, Kondziolka D, Lunsford LD, Kassam A, Phuong LK, Liscak R, et al. Development of a model to predict permanent symptomatic postradiosurgery injury for arteriovenous malformation patients. Int J Radiat Oncol Biol Phys 2000; 46–5:1143–8. https://doi.org/10.1016/s0360-3016(99)00513-1.
[53] Korytko T, Radivoyevitch T, Colussi V, Wessels BW, Pillai K, Maciunas RJ, et al. 12 Gy gamma knife radiosurgical volume is a predictor for radiation necrosis in non-avm intracranial tumors. Int J Radiat Oncol Biol Phys 2006;64–2:419–24. https://doi.org/10.1016/j.ijrobp.2005.07.980.